# Synchronized Energy and Electron Transfer Processes in Covalently Linked CdSe–Squaraine Dye–$TiO_2$ Light Harvesting Assembly

**Hyunbong Choi, Pralay K. Santra, and Prashant V. Kamat***

Radiation Laboratory and Department of Chemistry and Biochemistry, University of Notre Dame, Notre Dame, Indiana 46556, United States

**ABSTRACT** Manipulation of energy and electron transfer processes in a light harvesting assembly is an important criterion to mimic natural photosynthesis. We have now succeeded in sequentially assembling CdSe quantum dot (QD) and squaraine dye (SQSH) on $TiO_2$ film and couple energy and electron transfer processes to generate photocurrent in a hybrid solar cell. When attached separately, both CdSe QDs and SQSH inject electrons into $TiO_2$ under visible–near-IR irradiation. However, CdSe QD if linked to $TiO_2$ with SQSH linker participates in an energy transfer process. The hybrid solar cells prepared with squaraine dye as a linker between CdSe QD and $TiO_2$ exhibited power conversion efficiency of 3.65% and good stability during illumination with global AM 1.5 solar condition. Transient absorption spectroscopy measurements provided further insight into the energy transfer between excited CdSe QD and SQSH (rate constant of $6.7 \times 10^{10}$ $s^{-1}$) and interfacial electron transfer between excited SQSH and $TiO_2$ (rate constant of $1.2 \times 10^{11}$ $s^{-1}$). The synergy of covalently linked semiconductor quantum dots and near-IR absorbing squaraine dye provides new opportunities to harvest photons from selective regions of the solar spectrum in an efficient manner.

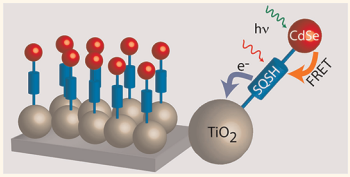


**KEYWORDS:** quantum dot solar cells · squaraine linker dye · photosensitization · transient absorption spectroscopy · photocurrent generation · CdSe

Increasing demand for clean energy and geopolitical complexity of fossil fuel dependence have prompted exploration of new and efficient solar energy conversion technologies.[1–4] Efforts are being made to mimic natural photosynthesis with sensitizing dyes and short band gap semiconductors. Of particular interest are the quantum-dot-sensitized solar cells (QDSCs) as they offer band gap tunability through size control.[5–11] Utilization of hot electrons and generation of mutiple charge carriers have made semiconductor quantum dots potentially important building blocks in light energy conversion devices.[12–15]

An essential requirement for efficient conversion of solar energy is a good spectral match between sensitizer absorption and incident solar radiation. Semiconductor quantum dots such as CdS and CdSe absorb only in the visible. Coupling with metal nanoparticles can extend the absorptivity and/or improved efficiency due to localized surface plasmons.[16,17] Another approach to maximize the absorption of incident photons would be to couple the short band gap semiconductor with an IR dye molecule.[18–21] The participation of both the semiconductor QD and the dye components in the solar cell resulted in cooperative photocurrent generation. Effective utilization of a QD as an antenna to capture photons and transfer energy to the sensitizing dye in a dye-sensitized solar cell (DSSC) is yet to be realized.

In recent years, a bifunctional linker molecule, HS–R–COOH, is widely used to link CdSe and $TiO_2$ nanoparticles.[22,23] The role of bifunctional surface modifiers, such as mercaptopropionic acid, in linking CdSe quantum dots (QDs) to mesoscopic $TiO_2$ films and its influence on the charge transfer kinetics have been elucidated.[24,25] Since such linker molecules do not absorb in the visible, they do not participate in the photoinduced electron transfer process. A careful design of a linker molecule with absorption in the near-IR region should enable capture of the photons over a wider spectral region. We have now employed a bifunctional squaraine dye as a linker since these classes of dyes are widely used to capture photons in the NIR region of dye-sensitized solar cells.[26–30] The squaraine dye (SQSH) thus serves dual functionality. First, the linker dye captures the NIR region of sunlight and sensitizes the mesoscopic $TiO_2$ film, and second, it provides a link between CdSe QDs and $TiO_2$ moieties. The experimental results that describe mechanistic

* Address correspondence to pkamat@nd.edu.

Received for review May 4, 2012 and accepted June 1, 2012.

**Published online June 01, 2012**
10.1021/nn301982e

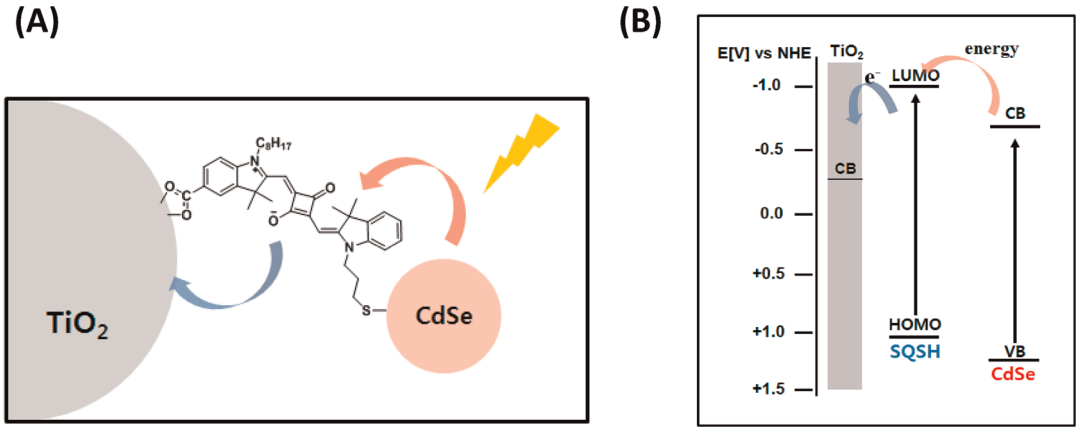


**Scheme 1. (A) Energy and electron transfer processes in $TiO_2$/SQSH/CdSe hybrid assembly (red arrow is the energy transfer from excited CdSe to SQSH, and blue arrow is the electron transfer from excited SQSH into $TiO_2$). (B) Energy level diagram illustrating sequential energy and electron processes in $TiO_2$/SQSH/CdSe under visible light irradiation.**

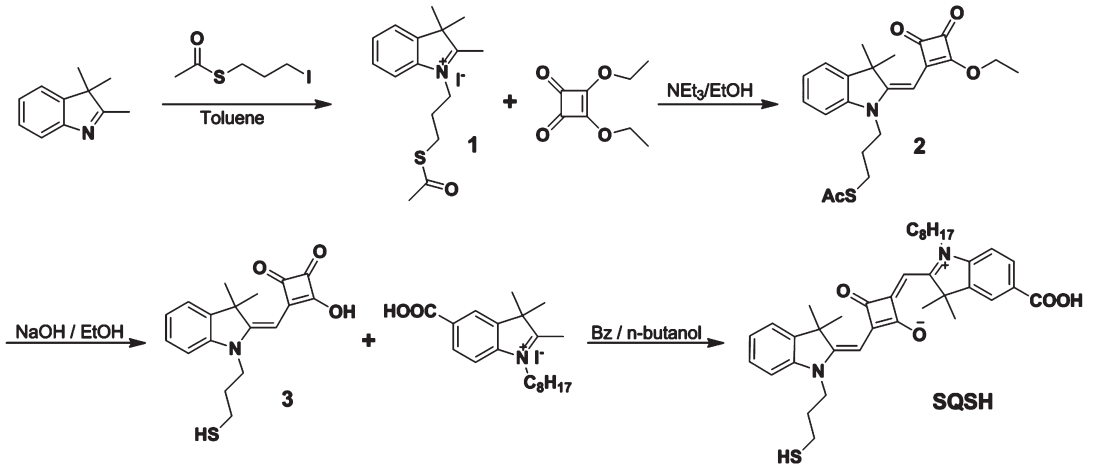


**Scheme 2. Synthetic strategy used for the NIR linker dye.**

and kinetic details of the energy and electron transfer in $TiO_2$/SQSH/CdSe hybrid assembly and their effective utilization in a hybrid solar cell are discussed in this article (Scheme 1).

## RESULTS AND DISCUSSION

**Synthesis of NIR Linker Molecule (SQSH).** The NIR linker dye SQSH was synthesized by the stepwise synthetic protocol as shown in Scheme 2. The (3-(acetylthio)-propyl)-2,3,3-trimethyl-3*H*-indolium iodide (**1**) was synthesized by the alkylation of 2,3,3-trimethylindolenin with 3-iodopropylthioacetate. The condensation of **1** with 3,4-diethoxy-3-cyclobutene-1,2-dione gave compound **2** in good yield. The hydrolysis of **2** with NaOH afforded hydroxymercaptopropylcyclobut-3-ene-1,2-dione derivative **3**. The condensation of **3** with 5-carboxy-2,3,3-trimethyl-1-octyl-3*H*-indolium was readily performed to give SQSH.

**Optical Properties of CdSe-Attached NIR Linker Dye.** Bifunctional linker molecules with carboxylate and thiol functional groups facilitate the binding of CdSe QDs to $TiO_2$. This approach has been found to be effective in linking size-selective semicondutor QDs to $TiO_2$[22] and gold[31,32] nanoparticles.

In the present study, we have used SQSH as the linker with a strong absorption in the red NIR region. We have also employed mercaptopropionic acid (MPA) as a reference to assess the effectiveness of the absorptive property of the linker dye. Modification of the $TiO_2$ film with SQSH and MPA was carried out by immersing the $TiO_2$ film in EtOH and acetonitrile solution of each linker for 12 h, respectively. The electrodes were then washed with EtOH to remove any excess physisorbed linkers and immersed in a toluene suspension of 3.4 nm diameter CdSe QDs. The thiol group binds strongly to CdSe nanoparticles. The carboxylate group of the linker facilitates the binding to $TiO_2$ nanoparticles. Figure 1 shows the absorption spectra of $TiO_2$ electrodes modified with CdSe and linker squaraine dye (SQSH). The absorption spectra of CdSe linked to MPA (MPA/CdSe) show typical absorption characteristics (*i.e.*, a sharp first excitonic peak ($1S_{3/2}1S_e$) at 550 nm with a broad second excitonic peak ($1P_{3/2}1P_e$) at 450 nm below 600 nm, corresponding

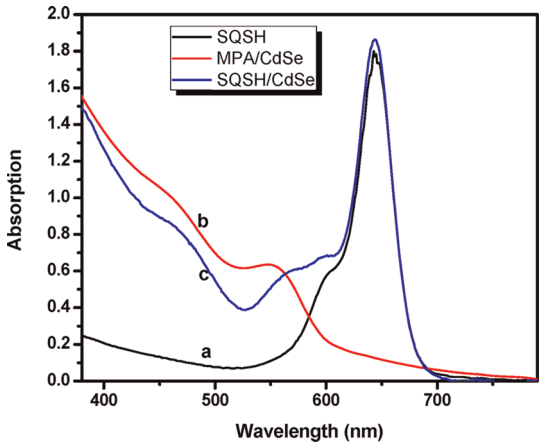


**Figure 1. Absorption spectra of (a) SQSH, (b) MPA/CdSe, and (c) SQSH/CdSe adsorbed onto $TiO_2$ films.**

to its band gap of ~2.0 eV). SQSH exhibits a prominent band in the red NIR region with a maximum at 640 nm. The linker dye exhibits relatively less absorption in the 400–550 nm region. The absorption spectra of CdSe linked to SQSH (SQSH/CdSe) exhibit strong absorption from the visible region to the red NIR region of sunlight, corresponding to both CdSe and linker dye. The small increase in optical density of the MPA/CdSe film at the CdSe region as compared to SQSH/CdSe arises from the difference of adsorbed amount of linker molecules due to different molecular size.

**Energy Transfer between Excited CdSe and SQSH.** The SQSH dye in the $TiO_2$/SQSH/CdSe hybrid assembly serves as a linker between $TiO_2$ and CdSe. When excited with visible light, the SQSH absorbs in the red NIR region while CdSe absorbs below 600 nm. Since these two components cover two different regions of the visible spectrum, we can selectively probe the contribution of each excitation event. First, we need to evaluate the interaction between excited CdSe and ground-state SQSH dye which is expected to dominate during visible excitation. The emission spectra of $SiO_2$ film modified with SQSH, MPA/CdSe, and SQSH/CdSe recorded following the excitation at 450 nm are shown in Figure 2. Since $SiO_2$ is an insulator, it does not participate in an electron transfer quenching process. The emission spectrum of SQSH deposited on $SiO_2$ (spectrum a) exhibits the characteristic emission band with a maximum at 670 nm. On the other hand, the emission spectrum of the CdSe QDs attached to $SiO_2$ exhibits characteristic band edge emission with a maximum at 570 nm (spectrum b). Upon linking CdSe QDs to linker dye (SQSH) on the $SiO_2$ surface, we observe more than 80% quenching of the CdSe emission (spectrum c). In parallel, we observe that an increase in the emission band of SQSH in spectrum c shows an enhancement with respect to the blank SQSH (spectrum a). Since we matched the absorbance at 450 nm, we expect to see minimal variation in the absorbed photons by these films. The quenching of the

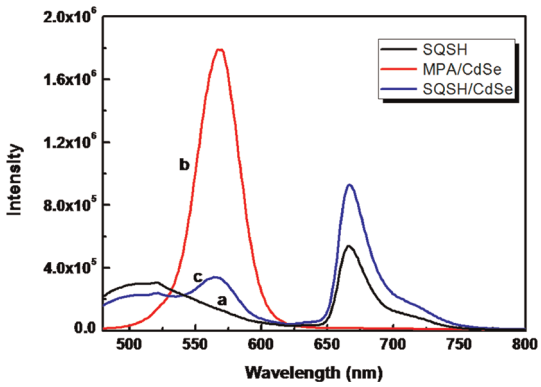


**Figure 2. Emission spectra of (a) SQSH, (b) MPA/CdSe, and (c) SQSH/CdSe deposited on $SiO_2$ film (excitation wavelength = 450 nm with matched absorbance for all three films).**

CdSe emission band and simultaneous increase in the emission of SQSH indicate that an energy transfer between excited CdSe and SQSH must be operative in SQSH/CdSe deposited on $SiO_2$ films. The overlap between CdSe emission and SQSH absorption and close proximity of the chemically linked donor and acceptor moieties make such an energy transfer possible. As indicated in the literature examples, excited CdSe is quite effective in transferring energy to dye molecules[33–36] and graphene.[37,38] For example, efficient Förster resonance energy transfer (FRET) by Mn- and Cu-doped semiconductor nanocrystal donors to organic dye acceptors (rhodamine B and cresyl violet) has been demonstrated.[39] Similarly, FRET has also been observed in electrostatically bound CdSe/ZnS quantum dot (QD)/J-aggregates of cyanine dye pairs.[40] Further evidence for the energy transfer between the excited CdSe and SQSH was obtained by recording excitation spectrum with emission being monitored at 670 nm. Increased emission response observed in the CdSe absorption region (400–580 nm) ascertains the role of CdSe as photon capturing antenna and transfer energy to SQSH (Supporting Information).

To further probe the interactive energy transfer between excited CdSe and SQSH, we investigated the dynamics of excited CdSe using transient absorption spectroscopy. The transient absorption spectra at different delay times and the bleaching recovery recorded following the excitation of MPA/CdSe and SQSH/CdSe linked to $SiO_2$ film are shown in Figure 3. In the case of the MPA/CdSe film, the spectra exhibit a strong bleach in the region of ground-state absorption. On the other hand, the difference absorption spectra of the SQSH/CdSe exhibit two strong bleaches arising from ground-state absorption of CdSe (550 nm) and SQSH (650 nm). The disappearance of ground-state bleaching in both CdSe and SQSH suggests the conversion of these two components into corresponding excited states. The bleaching recovery of the MPA/CdSe

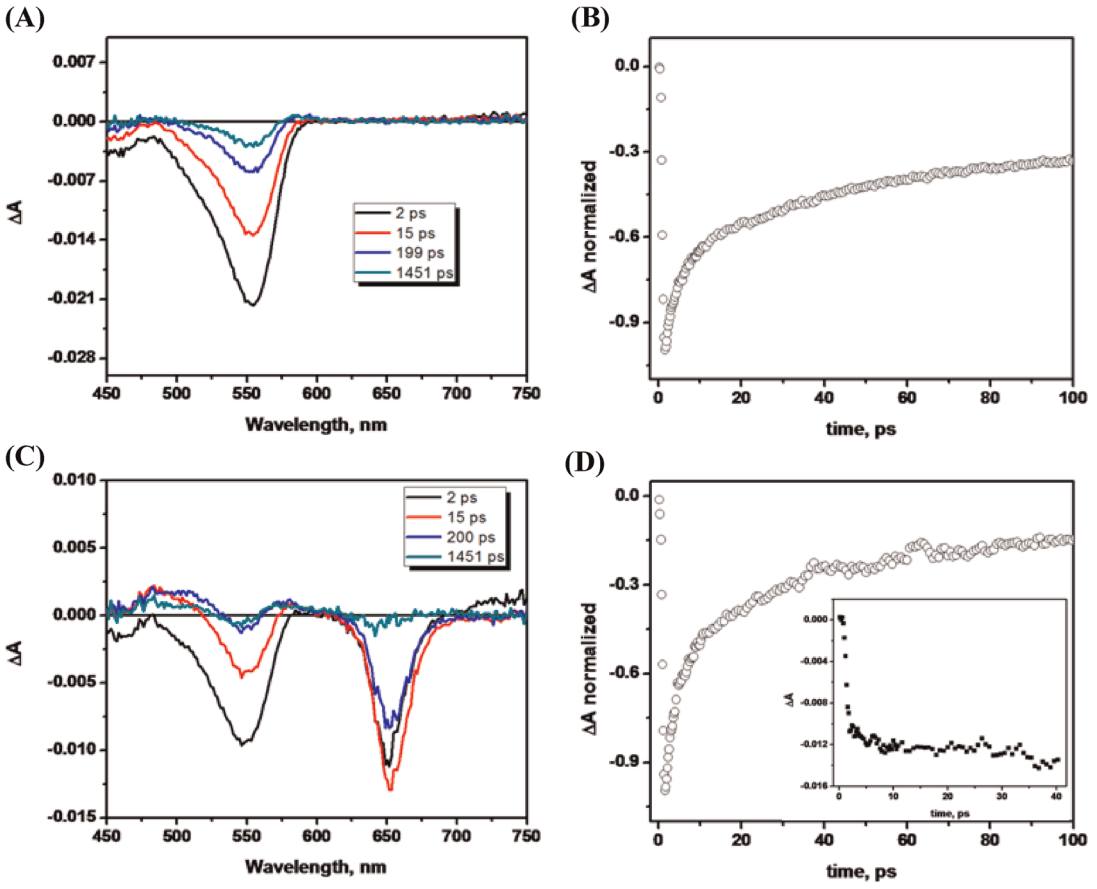


**Figure 3. Difference absorption spectra obtained upon femtosecond pump pulse (387 nm laser excitation) of (A) MPA/CdSe and (C) SQSH/CdSe on $SiO_2$ film. Time-absorption profiles of (B) MPA/CdSe and (D) SQSH/CdSe on $SiO_2$ film at 550 nm. Inset: time-absorption profiles of SQSH/CdSe on $SiO_2$ at 650 nm.**

shows multiexponential decay with recovery times stretched into nanoseconds. In the case of SQSH/CdSe, a faster component of the bleaching recovery is seen at 550 nm. The lifetime of this component corresponds to ~15 ps. If we attribute this fast recovery to the energy transfer to SQSH, we obtain a rate constant of energy transfer of $6.7 \times 10^{10}$ $s^{-1}$. Interestingly, this fast energy transfer is also seen in the bleaching of SQSH at 650 nm. The time-absorption profile recorded at 650 nm (inset of Figure 3D) shows a prompt rise followed by a slower growth in the bleaching signal during an initial period of 20 ps. The prompt bleaching arises from the direct excitation of the dye, while slow rise in the bleaching corresponds to the energy transfer component. These emission and transient absorption studies establish the role of SQSH as an effective interceptor for capturing energy from the excited CdSe. In the subsequent steps, the excited SQSH injects electrons into $TiO_2$ nanoparticles.

**Interaction between Excited SQSH and $TiO_2$.** The redox potential of the sensitizing dye provides a thermodynamic measure of the energetics of the ground and excited states. The oxidation potential of the SQSH as measured from the cyclic voltammogram (see Supporting Information) is around ~0.97 V *vs* NHE. The oxidation potential of the singlet excited SQSH calculated from the ground-state oxidation potential and the singlet energy (1.88 eV corresponding to the $E_{0\text{-}0}$ transition at 660 nm) corresponds to −0.91 V *vs* NHE. Thus, the excited SQSH is energetically capable of injecting electrons into the $TiO_2$ ($E_{CB}$ = −0.5 V *vs* NHE). However, the conduction band for CdSe in non-sulfide medium is around −0.70 V *vs* NHE.[41] Thus, there is relatively less driving force for the excited SQSH to induce electron transfer to CdSe. As a result of this energetic scheme, we expect the electron transfer between excited SQSH and $TiO_2$ to dominate following the visible excitation of the hybrid assembly, $TiO_2$/SQSH/CdSe.

Femtosecond transient absorption technique is a convenient approach to probe the ultrafast deactivation of excited dye on $TiO_2$ and other oxide surfaces.[42−44] In the present study, the dye (SQSH) was linked to mesoscopic $TiO_2$ and $SiO_2$ films. These two films were subjected to 387 nm laser pulse excitation in a pump−probe spectrophotometer, and the excited-state deactivation of the dye on the two oxide surfaces was compared (reactions 1 and 2).

$$SiO_2 - SQSH + h\nu \rightarrow SiO_2 - {}^1SQSH^* \rightarrow SiO_2 - SQSH + h\nu' \quad (1)$$

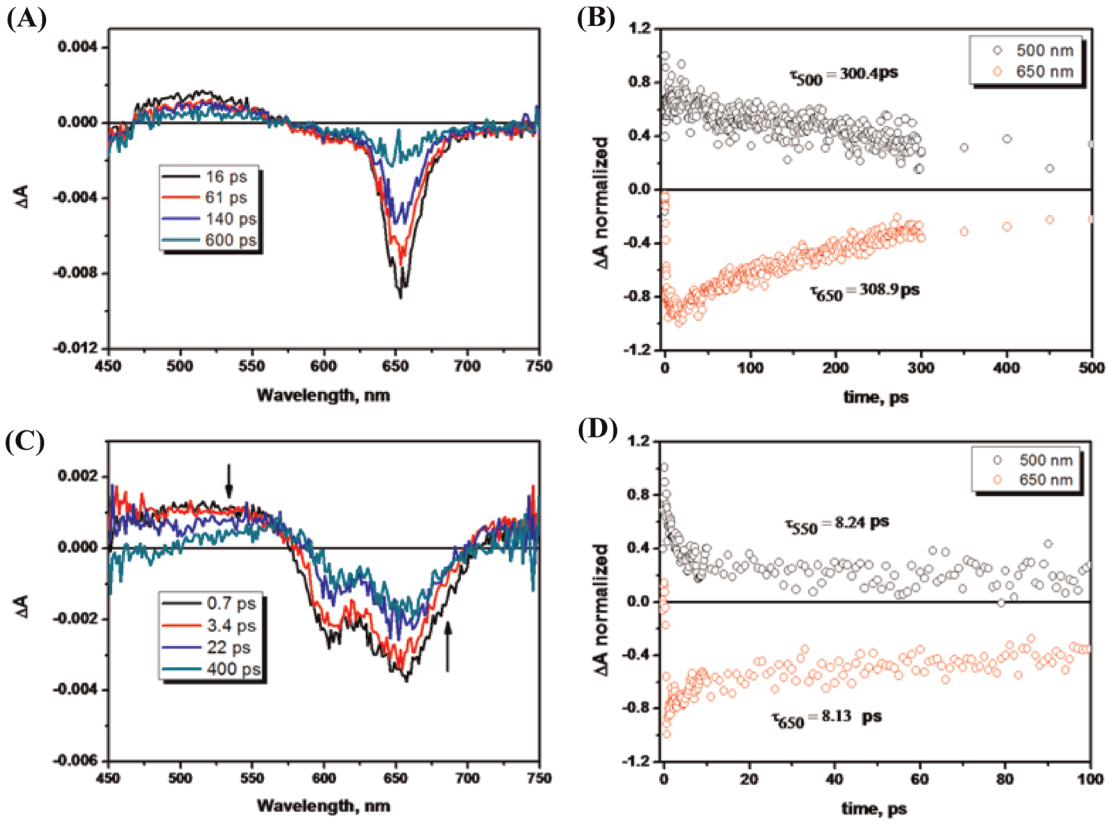


**Figure 4. Difference absorption spectra obtained upon femtosecond pump pulse (387 nm laser excitation) of (A) SQSH on $SiO_2$ and (C) SQSH on $TiO_2$ film. Time-absorption profiles of (B) SQSH on $SiO_2$ and (D) SQSH on $TiO_2$ film at 550 and 650 nm.**

$$TiO_2 - SQSH + h\nu \rightarrow TiO_2 - {}^1SQSH^* \rightarrow TiO_2(e) - SQSH^{+\bullet} \quad (2)$$

The transient absorption spectra recorded at different delay times following the laser pulse excitation of SQSH linked to $SiO_2$ and $TiO_2$ films are shown in Figure 4A,C. On $SiO_2$, the observed spectral fingerprints correspond to the singlet excited state with a bleaching at 640 nm and broad absorption around 520 nm. The lifetime of the SQSH* as monitored from the bleaching recovery and the decay of the transient absorption at 520 nm (Figure 4B) was ~300 ps. Since $SiO_2$ is an insulator, it does not directly participate in the electron transfer process. This is also evident from the single exponential decay kinetics of the excited state.

On the other hand, the difference absorption spectra of the SQSH linked to the $TiO_2$ film exhibit two absorption maxima around 550 nm and >725 nm and a broader bleach around 650 nm (Figure 4C). The transient decay as well as bleaching recovery (Figure 4C) exhibits a short and long-lived component. The fast component, which corresponds to singlet excited state of SQSH, decays with a lifetime of 8 ps. This faster decay represents deactivation of the excited state *via* a charge injection process (reaction 2). Indeed the long-lived component confirms the formation of cation radical of the dye following the charge injection into $TiO_2$. If we assume that the faster deactivation is entirely due to the electron injection process, we obtain a rate constant of $1.2 \times 10^{11}$ $s^{-1}$. Similar ultrafast electron injection rate constants have been reported for other dye sensitization of $TiO_2$ films.[45−47]

**Evaluation of QDSC Performance.** If indeed there is a synergy of energy and electron transfer processes in the $TiO_2$/SQSH/CdSe hybrid assembly, we should be able to observe its effectiveness during the operation of a photoelectrochemical solar cell. The mesoscopic $TiO_2$ films modified with SQSH, MPA/CdSe, and SQSH/CdSe were employed as photoanode, platinum counter electrode, and an electrolyte consisting of 0.22 M $Co(bpy)_3(PF_6)_2$, 0.033 M $Co(bpy)_3(PF_6)_3$, 0.1 M $LiClO_4$, and 0.2 M 4-*tert*-butylpyridine in acetonitrile.

The solar cell characteristics of the $TiO_2$ film modified with SQSH, MPA/CdSe, and SQSH/CdSe were recorded under AM 1.5 irradiation (100 mW $cm^{-2}$). Figure 5A shows the incident photon to current conversion efficiency (IPCE) or external quantum efficiency, and Figure 5B shows *J*−*V* characteristics of three different solar cells. The maximum IPCE for the solar cell employing SQSH alone corresponds to about 65% and matches the absorption band of the dye (maximum at 650 nm). On the other hand, the CdSe QDs attached to $TiO_2$ exhibit photoresponse below 530 nm with maximum IPCE of ~10% in the visible region. The SQSH/CdSe hybrid assembly on the other

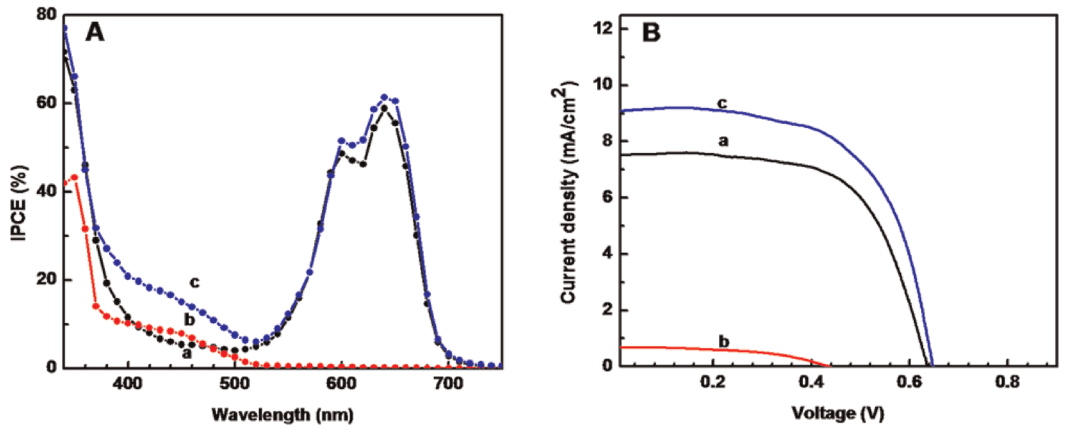


**Figure 5. (A) IPCE spectra and (B) *J*–*V* characteristics of (a) SQSH, (b) MPA/CdSe, and (c) SQSH/CdSe using Pt counter electrode and electrolyte of 0.22 M $Co(bpy)_3(PF_6)_2$, 0.033 M $Co(bpy)_3(PF_6)_3$, 0.1 M $LiClO_4$, and 0.2 M 4-*tert*-butylpyridine in acetonitrile.**

**TABLE 1. Solar Cell Performance Parameters[a]**

| dye | $J_{sc}$ (mAcm$^{-2}$) | $V_{oc}$ (V) | FF | $\eta$ (%) |
|---|---|---|---|---|
| SQSH | 7.525 | 0.637 | 0.64 | 3.05 |
| MPA/CdSe | 0.686 | 0.435 | 0.50 | 0.15 |
| SQSH/CdSe | 9.077 | 0.647 | 0.62 | 3.65 |

[a] Performances of QDSSCs were measured with 0.18 cm$^2$ working area. Electrolyte: 0.22 M $Co(bpy)_3(PF_6)_2$, 0.033 M $Co(bpy)_3(PF_6)_3$, 0.1 M $LiClO_4$, and 0.2 M 4-*tert*-butylpyridine in acetonitrile.

hand exhibits collective response throughout the visible region. Whereas the IPCE increase in the 650 nm is relatively small, significant increase in the IPCE is seen at wavelengths below 550 nm. This increase in IPCE of SQSH/CdS indicates the synergy of tapping energy and electron transfer processes by capturing the photons throughout the visible spectrum.

The *J*–*V* characteristics of the QDSC employing various photoanodes are presented in Figure 5B, and the cell parameters are summarized in Table 1. The open-circuit voltages of SQSH and SQSH/CdSe are similar, and it is greater than CdSe. A similar trend was also evident in the short-circuit current and fill factors. It is evident from the comparison of cell parameters (short-circuit current density ($J_{sc}$) of 9.07 mA cm$^{-2}$, open-circuit voltage ($V_{oc}$) of 647 mV, and fill factor (FF) of 0.62) that SQSH/CdSe exhibits superior performance. The power conversion efficiency ($\eta$) of 3.65% observed for the SQSH/CdSe hybrid solar cell was greater than the sum of solar cells employing SQSH (3.05%) or CdSe (0.15%) linked to $TiO_2$ as photoanodes. This enhanced efficiency observed during visible light illumination confirms the synergy of effective coupling energy and electron transfer processes in the hybrid solar cell.

## CONCLUSIONS

The property of CdSe quantum dots as light harvesting antenna has been successfully adopted in a covalently linked $TiO_2$/SQSH/$TiO_2$ hybrid assembly. The linker dye with its absorption in the red near-IR region couples CdSe QDs to $TiO_2$ and directly participates in the excited-state electron transfer process. The ability to capture energy from excited CdSe *via* FRET and to inject electrons into $TiO_2$ is reflected in the broader response of the solar cell with greater efficiency. The synergy of achieving sequential energy and electron transfer in a semiconductor–dye assembly seen in the present study opens new ways to capture a broader spectrum of incident photons and generate photocurrent in a solar cell with greater efficiency. A careful design of such hybrid assemblies that facilitate sequential energy and electron transfer processes could pave the way for developing new and efficient light harvesting assemblies.

## EXPERIMENTAL METHODS

**Materials.** All reactions were carried out under an argon atmosphere. Solvents were distilled from appropriate reagents. $Co(bpy)_3(PF_6)_2$ and $Co(bpy)_3(PF_6)_3$ were synthesized using the procedure described in the literature.[48] 3-Iodopropylthioacetate[49] and 5-carboxy-2,3,3-trimethyl-1-octyl-3*H*-indolium iodide[28] were synthesized using a modified procedure of previous references. The following materials were used for the synthesis of CdSe quantum dots. Cadmium oxide (CdO, Alfa, 99.998%), Se powder (Aldrich, 99.5%, 100 mesh), trioctylphosphine oxide (TOPO, Strem Chemicals, 90%), trioctylphosphine (TOP, Aldrich, 90%), and tetradecylphosphonic acid (TDPA, PCI Synthesis, lot# 808001N11) were used as received. $^1$H and $^{13}$C NMR spectra were recorded on a Varian Mercury 300 spectrometer.

**Optical and Electrochemical Measurements.** All experiments were carried out at room temperature. All solutions were deaerated by bubbling with nitrogen or argon. Absorption spectra were measured with a Varian Cary 50-Bio UV–vis spectrophotometer. Emission spectra were recorded using an SLM-S 8000 spectrofluorometer. A Princeton Applied Research model PARSTAT 2263 was used for recording *I*–*V* characteristics. Newport Oriel QE kit (QE-PV-SI) was used for measuring IPCE values. Cyclic voltammograms were recorded with a Gamry PC-14

potentiostat. A three-electrode system was used and consisted of a SCE, working electrode, and platinum wire electrode.

**Femtosecond Laser Flash Photolysis.** Femtosecond transient absorption experiments were conducted using a CPA-2010 1 kHz amplified Ti:sapphire laser system from Clark MXR, combined with Helios optical detection system provided by Ultrafast Systems. The fundamental output of the CPA-2010 laser system (775 nm, 1 mJ per pulse, pulse width 150 fs) was split into two beams: a pump (95%) and a probe (5%). The pump beam was directed through a second harmonic generator to provide 387 nm excitation wavelength. The probe beam passed through an optical delay rail, allowing regulation of an appropriate delay time between the pump and the probe.

**Solar Cell Fabrication.** The sensitized $TiO_2$ film is used as a working electrode. The FTO plate (Pilkington TEC Glass-TEC 8, Solar 2.3 mm thickness) used for the counter electrodes was cleaned with an ultrasonic bath in $H_2O$, acetone, and 0.1 M aqueous HCl, subsequently. Counter electrodes were prepared by coating with a drop of $H_2PtCl_6$ solution (2 mg of Pt in 1 mL of ethanol) on the cleaned FTO plate and sintered at 400 °C for 15 min. The dye-adsorbed $TiO_2$ electrode and Pt counter electrode were assembled into a sealed sandwich-type cell by heating at 80 °C with a hot-melt ionomer film (Surlyn SX 1170-25, Solaronix) as a spacer between the electrodes. A drop of electrolyte solution (electrolyte of 0.22 M $Co(bpy)_3(PF_6)_2$, 0.033 M $Co(bpy)_3(PF_6)_3$, 0.1 M $LiClO_4$, and 0.2 M 4-*tert*-butylpyridine in acetonitrile) was placed over a hole drilled in the counter electrode of the assembled cell and was driven into the cell *via* vacuum backfilling. Finally, the hole was sealed using additional Surlyn and a cover glass (0.1 mm thickness).

**1-(3-(Acetylthio)propyl)-2,3,3-trimethyl-3*H*-indolium iodide (1).** 3-Iodopropylthioacetate (1.2 g, 5.35 mmol) and 2,3,3-trimethylindolenin (0.852 g, 5.35 mmol) were dissolved in toluene and refluxed under nitrogen for 11 h. The solvent was evaporated, and the product was used without any further purification, 2.15 g (quantitative).

**(*E*)-(*S*)-3-(2-((2-Ethoxy-3,4-dioxocyclobut-1-enyl)methylene)-3,3-dimethylindolin-1-yl)propyl ethanethioate (2).** Compound **1** (1.64 g, 4.066 mmol), 3,4-diethoxy-3-cyclobutene-1,2-dione (0.577 g, 3.391 mmol), and 2 mL of triethylamine were dissolved in 25 mL of ethanol and refluxed for 30 min. The solvent was removed from the yellow solution, and the crude product was purified by recrystallization with ethanol to afford **2** in 70% yield. $^1$H NMR ($CDCl_3$): $\delta$ 7.29 (t, $J$ = 7.1 Hz, 1H), 7.27 (t, $J$ = 7.1 Hz, 1H), 7.08 (d, $J$ = 7.4 Hz, 1H), 6.92 (d, $J$ = 7.4 Hz, 1H), 5.41 (s, 1H), 4.90 (q, $J$ = 9.0 Hz, 2H), 3.89 (t, $J$ = 6.0 Hz, 2H), 2.96 (t, $J$ = 6.0 Hz, 2H), 2.38 (s, 3H), 2.04 (m, 2H), 1.62 (s, 6H), 1.55 (t, $J$ = 9.0 Hz, 3H). $^{13}$C{$^1$H} NMR ($CDCl_3$): $\delta$ 195.5, 187.9, 174.0, 168.3, 142.6, 141.0, 128.1, 123.0, 122.3, 108.4, 81.7, 70.2, 48.2, 41.8, 30.9, 27.2, 26.7, 26.5, 17.1, 16.2, 10.9.

**(*E*)-3-Hydroxy-4-((1-(3-mercaptopropyl)-3,3-dimethylindolin-2-ylidene)-methyl)cyclobut-3-ene-1,2-dione (3).** Compound **2** (0.4 g, 1.001 mmol) was dissolved in 40 mL of ethanol, and 2 mL of 1 M NaOH solution was added under reflux and heated for 20 min. The mixture was quenched with $H_2O$ (30 mL) and adjusted to pH 4 with 1 M HCl. The mixture was extracted with $CH_2Cl_2$ three times. The organic layer was separated and dried in $MgSO_4$. The solvent was removed *in vacuo*. The pure product was purified by recrystallization with ethanol to afford **3** in 60% yield. $^1$H NMR ($CDCl_3$): $\delta$ 7.28 (t, $J$ = 7.2 Hz, 1H), 7.26 (t, $J$ = 7.2 Hz, 1H), 7.07 (d, $J$ = 7.4 Hz, 1H), 6.93 (d, $J$ = 7.4 Hz, 1H), 5.40 (s, 1H), 2.96 (t, $J$ = 6.0 Hz, 2H), 2.58 (t, $J$ = 6.0 Hz, 2H), 2.04 (m, 2H), 1.62 (s, 6H). $^{13}$C{$^1$H} NMR ($CDCl_3$): $\delta$ 187.9, 174.0, 168.3, 142.6, 141.0, 128.1, 123.0, 122.3, 108.4, 81.7, 70.2, 48.2, 30.9, 27.2, 26.5, 17.1, 16.2.

**(*E*)-4-((5-Carboxy-3,3-dimethyl-1-octyl-3*H*-indolium-2-yl)methylene)-2-((*E*)-(1-(3-mercaptopropyl)-3,3-dimethylindolin-2-ylidene)methyl)-3-oxocyclobut-1-enolate (SQSH).** 3,5-Carboxy-2,3,3-trimethyl-1-octyl-3*H*-indolium iodide (0.56 g, 1.7 mmol) was dissolved in a mixture of 30 mL of benzene and 30 mL of *n*-butanol. The mixture was refluxed overnight. The solvent was removed *in vacuo*. The pure product SQSH was obtained by silica gel chromatography (eluent Mc/MeOH = 97:3, $R_f$ = 0.3) to afford SQSH in 71% yield. $^1$H NMR ($CDCl_3$): $\delta$ 8.05 (d, $J$ = 8.2 Hz, 1H), 7.21 (d, $J$ = 8.2 Hz, 1H), 8.01 (s, 1H), 7.51 (d, $J$ = 7.3 Hz, 1H), 7.27 (t, $J$ = 7.2 Hz, 1H), 7.41 (t, $J$ = 7.2 Hz, 1H), 7.33 (d, $J$ = 7.2 Hz, 1H), 6.08 (s, 1H), 5.94 (s, 1H), 4.24 (t, $J$ = 7.2 Hz, 2H), 4.09 (m, 2H), 2.43 (m, 3H), 1.82 (m, 2H), 1.80 (m, 2H), 1.76 (s, 6H), 1.75 (s, 6H), 1.46 (m, 2H), 1.31 (m, 2H), 1.3−1.4 (m, 4H), 1.29 (m, 2H), 0.88 (t, $J$ = 6.9 Hz, 3H). $^{13}$C{$^1$H} NMR ($CDCl_3$): $\delta$ 184.4, 179.4, 175.0, 173.9, 170.3, 169.8, 147.8, 143.5, 143.1, 142.9, 131.8, 129.3, 126.7, 126.3, 124.6, 123.4, 111.9, 110.3, 87.8, 87.6, 51.1, 49.6, 44.7, 40.0, 32.8, 30.6, 30.3, 30.4, 28.0, 27.8, 27.2, 26.9, 23.5, 22.4, 14.4, 12.5.

**Preparation of CdSe Colloids.** CdSe QDs were synthesized using a previous method.[50] In brief, 0.05 g of CdO, 0.3 g of TDPA, and 2 g of TOPO were heated in a three-neck round-bottom flask in nitrogen atmosphere. At 315 °C, a 4 mL of TOP and 0.25 mL of 1 M TOPSe (Se dissolved in TOP, prepared inside a glovebox) were injected swiftly to the reaction mixture. Heating was continued until the desired size of QDs has formed, evidenced by the color change of the reaction mixture. The growth was quenched by removing the heating source and carefully applying a wet paper towel on the reaction vessel wall. Once the solution reached below 80 °C, toluene was added and the reaction mixture was transferred to a glovebox under $N_2$ atmosphere. The QDs were precipitated by adding methanol. These particles were washed five times by suspending in toluene and subsequent addition of methanol to precipitate.

**Nanocrystalline $TiO_2$ Electrode Preparation.** FTO glass plates (Pilkington TEC Glass-TEC 8, Solar 2.3 mm thickness) were cleaned in a detergent solution using an ultrasonic bath for 30 min and rinsed with water and ethanol. The FTO glass plates were immersed in 40 mM $TiCl_4$ (aqueous) at 70 °C for 30 min and washed with water and ethanol. A transparent nanocrystalline layer on the FTO glass plate was prepared by doctor blade printing $TiO_2$ paste (Solaronix, Ti-Nanoxide T/SP) and then dried at 25 °C for 2 h. The $TiO_2$ electrodes were gradually heated under an air flow at 325 °C for 5 min, at 375 °C for 5 min, at 450 °C for 15 min, and at 500 °C for 15 min. A paste for the scattering layer containing 400 nm sized anatase $TiO_2$ particles (CCIC, PST-400C) was deposited by doctor blade printing and then dried for 2 h at 25 °C. The $TiO_2$ electrodes were again gradually heated under an air flow at 325 °C for 5 min, at 375 °C for 5 min, at 450 °C for 15 min, and at 500 °C for 15 min. The $TiO_2$ electrodes were treated again by $TiCl_4$ at 70 °C for 30 min and sintered at 500 °C for 30 min.

**Linking CdSe Nanocrystals to $TiO_2$ Films ($TiO_2$/MPA/CdSe and $TiO_2$/SQSH/CdSe).** After the treatment of $TiCl_4$, the $TiO_2$ films were placed directly into a 1 M 3-mercaptopropionic acid (MPA) in acetonitrile solution or 0.3 mM SQSH in EtOH for 12 h to allow for attachment of linker molecules. The films were subsequently washed with ethanol and placed directly in the CdSe nanoparticle solution ($\sim 8 \times 10^{-6}$ mol of dots/L) for 48 h.

**$TiO_2$/SQSH Film.** After the treatment of $TiCl_4$, the $TiO_2$ film was placed directly into a 0.3 mM SQSH in EtOH for 12 h to allow for attachment of linker molecules.

*Conflict of Interest:* The authors declare no competing financial interest.

*Acknowledgment.* The research described herein was supported by the Division of Chemical Sciences, Geosciences, and Biosciences, Office of Basic Energy Sciences of the U.S. Department of Energy through award DE-FC02-04ER15533. This is contribution number NDRL 4912 from the Notre Dame Radiation Laboratory.

*Supporting Information Available:* Excitation spectra and cyclic voltammetry of SQSH dye and the photocurrent response of MPA/CdSe and SQSH/CdSe electrodes to illumination are included in the Supporting Information. This material is available free of charge *via* the Internet at http://pubs.acs.org.

## REFERENCES AND NOTES

1. Kamat, P. V. Meeting the Clean Energy Demand: Nanostructure Architectures for Solar Energy Conversion. *J. Phys. Chem. C* **2007**, *111*, 2834–2860.
2. Kamat, P. V.; Tvrdy, K.; Baker, D. R.; Radich, J. G. Beyond Photovoltaics: Semiconductor Nanoarchitectures for Liquid Junction Solar Cells. *Chem. Rev.* **2010**, *110*, 6664–6688.

3. Walter, M. G.; Warren, E. L.; McKone, J. R.; Boettcher, S. W.; Mi, Q.; Santori, E. A.; Lewis, N. S. Solar Water Splitting Cells. *Chem. Rev.* **2010**, *110*, 6446–6473.
4. Maeda, K.; Domen, K. Photocatalytic Water Splitting: Recent Progress and Future Challenges. *J. Phys. Chem. Lett.* **2010**, *1*, 2655–2661.
5. Nozik, A. J. Quantum Dot Solar Cells. *Physica E* **2002**, *14*, 115–120.
6. Kamat, P. V. Quantum Dot Solar Cells. Semiconductor Nanocrystals as Light Harvesters. *J. Phys. Chem. C* **2008**, *112*, 18737–18753.
7. Mora-Sero, I.; Bisquert, J. Breakthroughs in the Development of Semiconductor Sensitized Solar Cells. *J. Phys. Chem. Lett.* **2010**, *1*, 3046–3052.
8. Buhbut, S.; Itzhakov, S.; Oron, D.; Zaban, A. Quantum Dot Antennas for Photoelectrochemical Solar Cells. *J. Phys. Chem. Lett.* **2011**, *2*, 1917–1924.
9. Hetsch, F.; Xu, X.; Wang, H.; Kershaw, S. V.; Rogach, A. L. Semiconductor Nanocrystal Quantum Dots as Solar Cell Components and Photosensitizers: Material, Charge Transfer, and Separation Aspects of Some Device Topologies. *J. Phys. Chem. Lett.* **2011**, *2*, 1879–1887.
10. Kramer, I. J.; Sargent, E. H. Colloidal Quantum Dot Photovoltaics: A Path Forward. *ACS Nano* **2011**, *5*, 8506–8514.
11. Yu, X.-Y.; Liao, J.-Y.; Qiu, K.-Q.; Kuang, D.-B.; Su, C.-Y. Dynamic Study of Highly Efficient CdS/CdSe Quantum Dot-Sensitized Solar Cells Fabricated by Electrodeposition. *ACS Nano* **2011**, *5*, 9494–9500.
12. Pandey, A.; Guyot-Sionnest, P. Hot Electron Extraction from Colloidal Quantum Dots. *J. Phys. Chem. Lett.* **2010**, *1*, 45–47.
13. Semonin, O. E.; Luther, J. M.; Choi, S.; Chen, H. Y.; Gao, J. B.; Nozik, A. J.; Beard, M. C. Peak External Photocurrent Quantum Efficiency Exceeding 100% *via* MEG in a Quantum Dot Solar Cell. *Science* **2011**, *334*, 1530–1533.
14. McGuire, J. A.; Joo, J.; Pietryga, J. M.; Schaller, R. D.; Klimov, V. I. New Aspects of Carrier Multiplication in Semiconductor Nanocrystals. *Acc. Chem. Res.* **2008**, *41*, 1810–1819.
15. Beard, M. C. Multiple Exciton Generation in Semiconductor Quantum Dots. *J. Phys. Chem. Lett.* **2011**, *2*, 1282–1288.
16. Choi, H.; Chen, W. T.; Kamat, P. V. Know Thy Nano Neighbor. Plasmonic *versus* Electron Charging Effects of Gold Nanoparticles in Dye Sensitized Solar Cells. *ACS Nano* **2012**, *6*, 4418–4427.
17. Hägglund, C.; Apell, S. P. Plasmonic Near-Field Absorbers for Ultrathin Solar Cells. *J. Phys. Chem. Lett.* **2012**, *3*, 1275–1285.
18. Hotchandani, S.; Kamat, P. V. Modification of Electrode Surface with Semiconductor Colloids and Its Sensitization with Chlorophyll *a*. *Chem. Phys. Lett.* **1992**, *191*, 320–326.
19. Choi, H.; Nicolaescu, R.; Paek, S.; Ko, J.; Kamat, P. V. Supersensitization of CdS Quantum Dots with NIR Organic Dye: Towards the Design of Panchromatic Hybrid-Sensitized Solar Cells. *ACS Nano* **2011**, *5*, 9238–9245.
20. Shalom, M.; Albero, J.; Tachan, Z.; Martinez-Ferrero, E.; Zaban, A.; Palomares, E. Quantum Dot-Dye Bilayer-Sensitized Solar Cells: Breaking the Limits Imposed by the Low Absorbance of Dye Monolayers. *J. Phys. Chem. Lett.* **2010**, *1*, 1134–1138.
21. Buhbut, S.; Itzhakov, S.; Tauber, E.; Shalom, M.; Hod, I.; Geiger, T.; Garini, Y.; Oron, D.; Zaban, A. Built-in Quantum Dot Antennas in Dye-Sensitized Solar Cells. *ACS Nano* **2010**, *4*, 1293–1298.
22. Robel, I.; Subramanian, V.; Kuno, M.; Kamat, P. V. Quantum Dot Solar Cells. Harvesting Light Energy with CdSe Nanocrystals Molecularly Linked to Mesoscopic $TiO_2$ Films. *J. Am. Chem. Soc.* **2006**, *128*, 2385–2393.
23. Watson, D. F. Linker-Assisted Assembly and Interfacial Electron-Transfer Reactivity of Quantum Dot Substrate Architectures. *J. Phys. Chem. Lett.* **2010**, *1*, 2299–2309.
24. Hyun, B.-R.; Bartnik, A. C.; Sun, L.; Hanrath, T.; Wise, F. W. Control of Electron Transfer from Lead-Salt Nanocrystals to $TiO_2$. *Nano Lett.* **2011**, *11*, 2126–2132.
25. Pernik, D.; Tvrdy, K.; Radich, J. G.; Kamat, P. V. Tracking the Adsorption and Electron Injection Rates of CdSe Quantum Dots on $TiO_2$: Linked *versus* Direct Attachment. *J. Phys. Chem. C* **2011**, *115*, 13511–13519.
26. Ko, J.; Paek, S.; Choi, H.; Kim, C.; Cho, N.; So, S.; Song, K.; Nazeeruddin, M. K. Efficient and Stable Panchromatic Squaraine Dyes for Dye-Sensitized Solar Cells. *Chem. Commun.* **2011**, *47*, 2874–2876.
27. Paek, S.; Choi, H.; Kim, C.; Cho, N.; So, S.; Song, K.; Nazeeruddin, M. K.; Ko, J. Efficient and Stable Panchromatic Squaraine Dyes for Dye-Sensitized Solar Cells. *Chem. Commun.* **2011**, *47*, 2874–2876.
28. Yum, J. H.; Walter, P.; Huber, S.; Rentsch, D.; Geiger, T.; Nuesch, F.; De Angelis, F.; Gratzel, M.; Nazeeruddin, M. K. Efficient Far Red Sensitization of Nanocrystalline $TiO_2$ Films by an Unsymmetrical Squaraine Dye. *J. Am. Chem. Soc.* **2007**, *129*, 10320–10321.
29. Das, S.; George-Thomas, K.; Kamat, P. V.; George, M. V. Photosensitizing Properties of Squaraine Dyes. *Proc. Indiana Acad. Sci.* **1993**, *105*, 513–525.
30. Wojcik, A.; Nicolaescu, R.; Kamat, P. V.; Patil, S. Photochemistry of Far Red Responsive Tetrahydroquinoxaline-Based Squaraine Dyes. *J. Phys. Chem. A* **2010**, *114*, 2744–2750.
31. Zayats, M.; Kharitonov, A. B.; Pogorelova, S. P.; Lioubashevski, O.; Katz, E.; Willner, I. Probing Photoelectrochemical Processes in Au−CdS Nanoparticle Arrays by Surface Plasmon Resonance: Application for the Detection of Acetylcholine Esterase Inhibitors. *J. Am. Chem. Soc.* **2003**, *125*, 16006–16014.
32. Kamat, P. V.; Barazzouk, S.; Hotchandani, S. Electrochemical Modulation of Fluorophore Emission at a Nanostructured Gold Film. *Angew. Chem., Int. Ed.* **2002**, *41*, 2764–2767.
33. Curutchet, C.; Franceschetti, A.; Zunger, A.; Scholes, G. D. Examining Forster Energy Transfer for Semiconductor Nanocrystalline Quantum Dot Donors and Acceptors. *J. Phys. Chem. C* **2008**, *112*, 13336–13341.
34. Dorokhin, D.; Hsu, S. H.; Tomczak, N.; Blum, C.; Subramaniam, V.; Huskens, J.; Reinhoudt, D. N.; Velders, A. H.; Vancso, G. J. Visualizing Resonance Energy Transfer in Supramolecular Surface Patterns of $\beta$-CD-Functionalized Quantum Dot Hosts and Organic Dye Guests by Fluorescence Lifetime Imaging. *Small* **2010**, *6*, 2870–2876.
35. Kowerko, D.; Schuster, J.; Amecke, N.; Abdel-Mottaleb, M.; Dobrawa, R.; Wurthner, F.; von Borczyskowski, C. FRET and Ligand Related Non-FRET Processes in Single Quantum Dot-Perylene Bisimide Assemblies. *Phys. Chem. Chem. Phys.* **2010**, *12*, 4112–4123.
36. Sadhu, S.; Haldar, K. K.; Patra, A. Size Dependent Resonance Energy Transfer between Semiconductor Quantum Dots and Dye Using FRET and Kinetic Model. *J. Phys. Chem. C* **2010**, *114*, 3891–3897.
37. Chen, Z.; Berciaud, S. P.; Nuckolls, C.; Heinz, T. F.; Brus, L. E. Energy Transfer from Individual Semiconductor Nanocrystals to Graphene. *ACS Nano* **2010**, *4*, 2964–2968.
38. Lightcap, I. V.; Kamat, P. V. Fortification of CdSe Quantum Dots with Graphene Oxide. Excited State Interactions and Light Energy Conversion. *J. Am. Chem. Soc.* **2012**, *134*, 7109–7116.
39. Sarkar, S.; Bose, R.; Jana, S.; Jana, N. R.; Pradhan, N. Doped Semiconductor Nanocrystals and Organic Dyes: An Efficient and Greener FRET System. *J. Phys. Chem. Lett.* **2010**, *1*, 636–640.
40. Halpert, J. E.; Tischler, J. R.; Nair, G.; Walker, B. J.; Liu, W.; Bulovic□, V.; Bawendi, M. G. Electrostatic Formation of Quantum Dot/J-Aggregate FRET Pairs in Solution. *J. Phys. Chem. C* **2009**, *113*, 9986–9992.
41. Ellis, A. B.; Kaiser, S. W.; Bolts, J. M.; Wrighton, M. S. Study of n-Type Semiconducting Cadmium Chalcogenide-Based Photoelectrochemical Cells Employing Polychalcogenide Electrolytes. *J. Am. Chem. Soc.* **1977**, *99*, 2839–2848.
42. Hannappel, T.; Burfeindet, B.; Storck, W.; Willig, F. Measurement of Ultrafast Photoinduced Electron Transfer from Chemically Anchored Ru-Dye Molecules into Empty Electronic States in a Colloidal Anatase $TiO_2$ Film. *J. Phys. Chem. B* **1997**, *101*, 6799–6802.

43. Ellingson, R. J.; Asbury, J. B.; Ferrere, S.; Ghosh, H. N.; Sprague, J. R.; Lian, T.; Nozik, A. J. Dynamics of Electron Injection in Nanocrystalline Titanium Dioxide Films Sensitized with [Ru(4,4′-dicarboxy-2,2′-bipyridine)$_2$ (NCS)$_2$] by Infrared Transient Absorption. *J. Phys. Chem. B* **1998**, *102*, 6455–6458.
44. Liu, D.; Kamat, P. V.; Thomas, K. G.; Thomas, K. J.; Das, S.; George, M. V. Picosecond Dynamics of an IR Sensitive Squaraine Dye. Role of Singlet and Triplet Excited States in the Photosensitization of $TiO_2$ Nanoclusters. *J. Chem. Phys.* **1997**, *106*, 6404–6410.
45. Rehm, J. M.; McLendon, G. L.; Nagasawa, Y.; Yoshihara, K.; Moser, J.; Grätzel, M. Femtosecond Electron-Transfer Dynamics at a Sensitizing Dye-Semiconductor ($TiO_2$) Interface. *J. Phys. Chem.* **1996**, *100*, 9577–9578.
46. Asbury, J. B.; Hao, E.; Wang, Y.; Lian, T. Bridge Length-Dependent Ultrafast Electron Transfer from Re Polypyridyl Complexes to Nanocrysalline$TiO_2$ Thin Films Studied by Femtosecond Infrared Spectroscopy. *J. Phys. Chem. B* **2000**, *104*, 11957–11964.
47. Asbury, J. B.; Wang, Y. Q.; Lian, T. Multiple-Exponential Electron Injection in Ru(dcbpy)$_2$(SCN)$_2$ Sensitized ZnO Nanocrystalline Thin Films. *J. Phys. Chem. B* **1999**, *103*, 6643–6647.
48. Feldt, S. M.; Gibson, E. A.; Gabrielsson, E.; Sun, L.; Boschloo, G.; Hagfeldt, A. Design of Organic Dyes and Cobalt Polypyridine Redox Mediators for High-Efficiency Dye-Sensitized Solar Cells. *J. Am. Chem. Soc.* **2010**, *132*, 16714–16724.
49. Kitagawa, T.; Dey, A.; Lugo-Mas, P.; Benedict, J. B.; Kaminsky, W.; Solomon, E.; Kovacs, J. A. A Functional Model for the Cysteinate-Ligated Non-Heme Iron Enzyme Superoxide Reductase (SOR). *J. Am. Chem. Soc.* **2006**, *128*, 14448–14449.
50. Peng, Z. A.; Peng, X. Formation of High-Quality CdTe, CdSe, and CdS Nanocrystals Using CdO as Precursor. *J. Am. Chem. Soc.* **2001**, *123*, 183–184.